Radiographic and Biomechanical Assessment of Three Implant Designs for Canine Cementless Total Hip Replacement

Natalie J. Worden[1] Kristian J. Ash[1] Nathaniel R. Ordway[2] Mark A. Miller[2] Kenneth A. Mann[2] Gretchen M. VanDeventer[1] Dominick M. Valenzano[1] Robert Hart[3] Mitsunori Kayano[4] Kei Hayashi[1]

[1] Department of Clinical Sciences, College of Veterinary Medicine, Cornell University, Ithaca, New York, United States
[2] Department of Orthopedic Surgery, SUNY Upstate Medical University, Syracuse, New York, United States
[3] Department of Orthopedic Surgery, Animal Medical Center, New York, New York, United States
[4] Department of Veterinary Medicine, Research Center for Global Agromedicine, Obihiro University of Agriculture and Veterinary Medicine, Obihiro, Japan

Address for correspondence Kei Hayashi, DVM, PhD, Department of Clinical Sciences, College of Veterinary Medicine, Cornell University, 930 Campus Road, Ithaca, NY 14850, United States (e-mail: kh528@cornell.edu).

Vet Comp Orthop Traumatol 2020;33:417–427.

Abstract

Objective The aim of this study was to evaluate the relationship between radiographic fit/fill measurements and biomechanical performance of three canine cementless total hip implant designs using an *in vitro* biomechanical testing protocol that replicates compression and torsion.

Study Design Eighteen (six/group) canine cadaveric femurs were implanted with one of three cementless total hip implant designs: (1) collarless, (2) collared or (3) lateral bolt stems. Femoral length, canal flare index (CFI), canal fill, stem fit, stem level and stem angle were measured as independent variables. Biomechanical performance was tested using physiological, non-destructive gait loading (*loading protocols*) and destructive testing (*failure protocols*).

Results During loading protocols, compressive stiffness was influenced by stem level ($p < 0.05$) and torsional stiffness was influenced by stem level and CFI for collarless stems ($p < 0.05$). During failure protocols, peak load was influenced by mediolateral (ML) stem angle ($p < 0.05$) and CFI ($p < 0.01$) for collarless stems and CFI for lateral bolt stems ($p < 0.05$). Peak torque was influenced by ML stem angle, craniocaudal stem angle and CFI for collarless stems ($p < 0.05$) and average ML fill for collared stems ($p < 0.05$).

Conclusion Biomechanical performance of collarless stems in cementless hip arthroplasty is more impacted by radiographic fit/fill than lateral bolt and collared stems. As a result, collarless stems may be more dependent on preoperative fit and intraoperative precision.

Keywords
- hip arthroplasty
- cementless
- radiograph
- biomechanics
- canine femur

received
November 7, 2019
accepted after revision
June 23, 2020
published online
September 24, 2020

DOI https://doi.org/10.1055/s-0040-1715476.
ISSN 0932-0814.

Introduction

Canine total hip replacement is a common treatment modality for coxofemoral osteoarthritis secondary to canine hip dysplasia, avascular necrosis of the femoral head and traumatic hip luxations.[1–6] In canine patients, rapid return to weight bearing and difficulty in moderating postoperative loading environments necessitates a high degree of initial stability. Although various techniques and implant systems have been devised, cementless canine total hip replacement systems were developed because they potentially offer improved long-term outcomes and greater resistance to infection than their cemented counterparts. These cementless systems, however, still have their own associated complications, including fractures and fissures, coxofemoral luxation, subsidence, implant loosening and failure of fixation.[7–11]

Cementless femoral stems typically rely on friction between the implant and bone for initial stability, which relates to both the shape of the femoral stem and the interface frictional forces present. Many factors influence this interaction, including surface roughness, accuracy of bone bed preparation and implant alignment, implantation force and patient activity and weight.[7] After implantation, a cementless femoral stem must remain stable for bone ingrowth to occur. 'Stability' has been shown to require $< 150\,\mu m$ of motion at the implant–bone interface.[8,9] A lack of implant stability may result in subsidence, or a distal sinking of the stem into the medullary canal. This has been commonly reported as a complication with the BFX total hip replacement system; however, many instances of implant subsidence are not associated with a negative clinical impact.[7,11]

Differences in femoral conformation also influence implant stability. Fixation of cementless femoral components in femoral geometries with a 'stove pipe' morphology (femoral canal flare index (CFI) of ≤ 1.8) is clinically challenging due to the lack of taper-lock between implant and endosteal bone surface.[10] This has been shown to contribute to instability and failure of the femoral component, making traditional tapered implants less suited for certain dog breeds that are predisposed to these anatomical environments.[10] To address this, various design iterations have been developed, including augmentation of the stem with a collar, a lateral bolt that engages the cortex or a short stem design that maintains more of the femoral neck.[12–14]

Previous *in vitro* test models of canine cementless hip implants have examined biomechanical parameters such as subsidence, stiffness, yield and failure under physiological loading conditions for either compression or torsion.[12,14,15] However, another study determined that *in vivo* loading of the canine hip involves both compressive and torsional components.[16] Therefore, our study applied an *in vitro* biomechanical test protocol evaluating both compression and torsion for experimental evaluation of canine cementless hip arthroplasty, which would be more representative of the physiological loading that occurs in the dog. The purpose of our study was to examine the mechanical performance of two implant augmentations compared with a traditional collarless-tapered stem and determine how the radiographic fit and fill parameters of all three implant styles would affect their performance. The null hypothesis was that implant design modifications would not affect mechanical properties predicted by radiographic measurements. The specific aim was to evaluate whether neutral stem angulation and maximal canal fill, as determined by radiographic measurements, would result in improved mechanical performance, including increased stiffness, peak load and peak torque.

Materials and Methods

Specimens and Preparation

Eighteen cadaveric femurs were collected from purpose bred research hound dogs (24–28 kg) humanely euthanatized for unrelated Institutional Animal Care and Use Committee approved studies. Dogs of this size were selected because they generally fit stems of sizes 8 and 9, which are commonly used in clinical practice.[11,17] Sample size was selected based on the availability of cadaveric femurs at the time of the study. The femurs were randomly assigned to one of three stem system treatment groups using GraphPad randomizer (GraphPad Software Inc, La Jolla, California, United States, http://www.graphpad.com/quickcalcs/randomize1.cfm).

Stem systems used in the treatment groups (collarless, collared and collarless with a lateral bolt) were all commercially available for clinical use at the time of testing (BFX cementless femoral implant, BioMedtrix; Whippany, New Jersey, United States) (►**Fig. 1**). All stems used in the study had an electron beam melting surface that was consistent in extent, structure and geometry across all implant types. The collarless stem was the standard titanium, long stem, single taper design. The collared stem features a medial collar at the base of the implant neck that follows the rounded medial calcar osteotomy line. The collarless stem with a lateral bolt has a 1.6 mm diameter hole through the centre of the neck and a 4.5 mm titanium bolt which locks into the prosthesis and engages the lateral cortex of the femur. All implanted stems were of sizes 8 and 9 and all lateral bolts were of large size.

All soft tissues were removed from the femurs via dissection and the femurs were radiographed in mediolateral (ML) and craniocaudal (CC) projections. The cadaveric femurs were wrapped in saline (0.9% NaCl) solution-soaked towels and frozen at –20°C. On the day of implantation, the femurs were thawed in a warm water bath. Each femur was size templated for the corresponding implant system using the manufacturer's supplied templates (BioMedtrix). The femurs were each implanted, in a random order, with their corresponding implant according to technique guidelines set forth by the manufacturer (►**Fig. 2**).[18–20] A boarded surgeon experienced with total hip replacements performed or supervised every implantation (KH). Supervised implantations were performed by a surgical resident (KJA). Orthogonal view radiographs were then repeated and the femurs were examined grossly to ensure proper implant placement (including collar-calcar contact for collared stems) and that no femoral fissure formation had occurred.

Fig. 1 Pre-implantation image of the three different cementless BFX femoral implants. From left to right: collarless, collared and lateral bolt.

Fig. 2 Radiographic comparison of implants. From left to right: an intact femur demonstrating canal flare index measurements, collarless implant, collared implant and lateral bolt implant.

Biomechanical Testing Protocols

Biomechanical testing was performed as previously described.[18] Briefly, the distal end of each femur was sectioned at 125 mm and potted in poly(methyl methacrylate) and consistent samples of 100 mm in length were placed in a biaxial materials testing machine (model 858; MTS, Eden Prairie, Minnesota, United States). Two protocols using combined loading (compression and torsion) were developed—a non-destructive protocol using load limits based on the peak forces during canine gait and a failure protocol using displacement limits that were 30 times the peak forces of canine gait.[16] Determination of displacement limits for the failure protocol was performed through pilot testing, as previously described.[18] The non-destructive protocol consisted of 10 cycles of preconditioning at 0.25 Hz and peak loads of 430 N compression and 1.6 Nm torsion. A final cycle was run for data collection. The failure protocol consisted of loading rates of 12 mm/min and 42 degrees/min of compression and torsion respectively. Data were collected up to the displacement limits of 6 mm and 21 degrees for compression and torsion respectively. For each protocol, data were collected for both compressive load/displacement and torsional torque/rotation. Stiffness values of compression and torsion were analysed for the non-destructive and failure tests. Orthogonal view radiographs were repeated to evaluate the femurs and implants post-failure.

Radiographic Analysis

Radiographic measurements were taken from preoperative and postoperative radiographs using the Carestream Vue PACS software (Carestream Health; Inc. 2013, Rochester, New York, United States). Measurements were performed by one investigator (NJW), and each measurement was repeated five times and averaged to compensate for variability in the measurements across different levels of magnification. Radiographs consisted of *ex vivo* canine femurs in CC and ML projections and were calibrated using a 100 mm bar. Femoral shape was assessed in terms of CFI and femoral length using the preoperative radiographs (►**Figs. 2** and **3**). Postoperative, pre-biomechanical testing radiographs were used to measure stem angulation, canal fill and stem level (►**Fig. 3**). The CFI, stem level and femur length were measured on the CC projection only. For the collared stems, the gap between the collar and calcar, if present, was measured on the CC projection. Femoral measurements were modelled after the methods described in prior studies.[17,21]

Canal fill was measured as the average ratio of implant width to femoral canal width at 5 mm, 15 mm and 25 mm from the distal tip of the implant stem on both the CC and ML projections, which were then averaged to determine the average canal fill for each femur on orthogonal planes.[17] The ML projection was used to calculate average CC fill and the CC projection was used to calculate average ML Fill. For stem angulation, varus/medial tipping and valgus/lateral tipping were assessed on the CC projection (ML stem angle) and determined based on the orientation of the distal implant stem. Cranial and caudal tipping were evaluated on the ML projection (CC stem angle) and were also determined based on the orientation of the distal implant stem. Stem level was measured as the distance between the shoulder of the implant and the most proximal aspect of the greater trochanter, and was then normalized by the total femoral length to account for anatomic variations in greater trochanter height. Postoperative radiographs were also used to evaluate stem fit on both the CC and ML projections. Assessment of stem fit was performed using a modified version of a previously described method.[22] Type 1 fit indicated that an implant made contact with the femoral cortex proximal to or within the region of the lesser

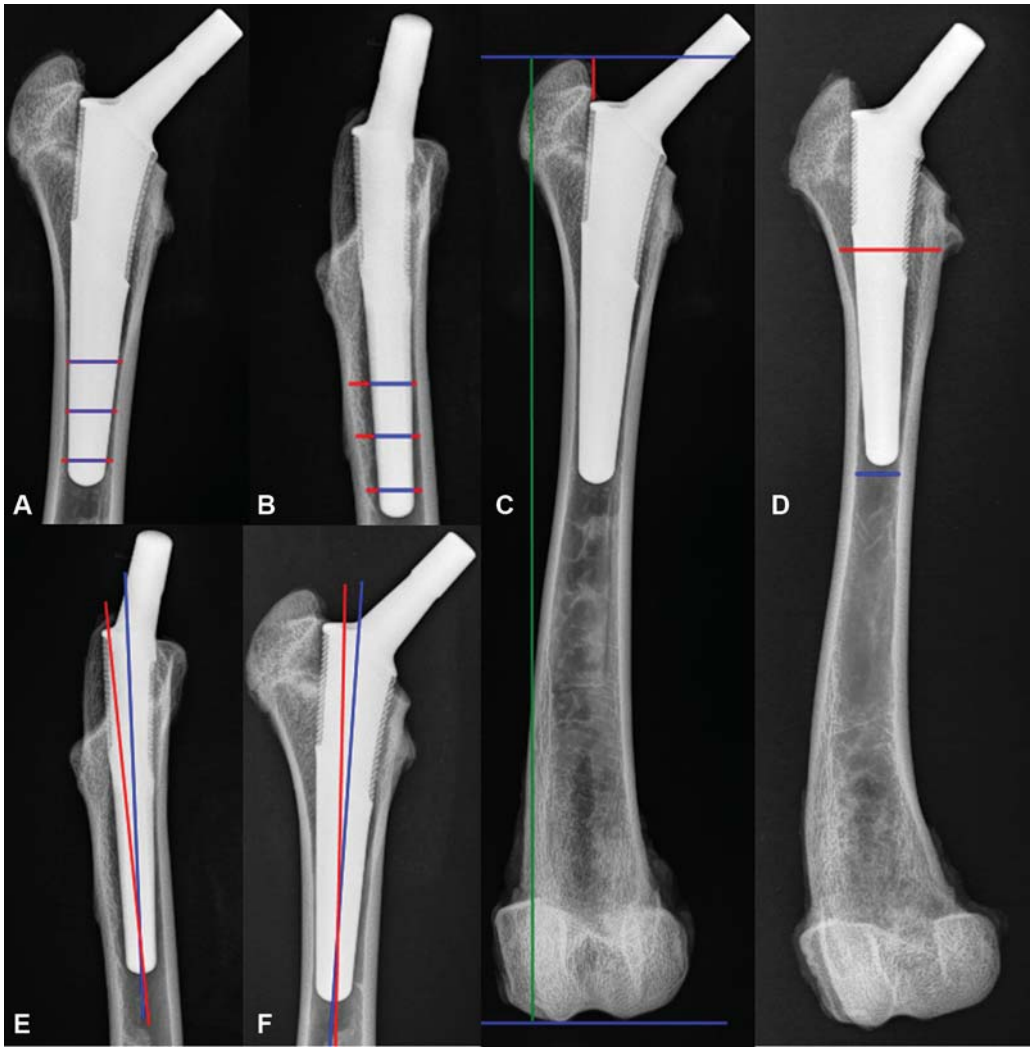

Fig. 3 Radiographic measurements of stem orientation. (**A**) Mediolateral canal fill was calculated at each level by dividing the implant width (blue line) by the canal width (red lines plus corresponding blue line) on the craniocaudal projection. (**B**) Craniocaudal canal fill was calculated at each level by dividing the implant width (blue line) by the canal width (red lines plus corresponding blue line) on the mediolateral projection. (**C**) Stem level (red line) was measured as the distance between the lateral shoulder of the implant and the level of the most proximal aspect of the greater trochanter, and was normalized by the femoral length (green line) which was measured as the distance between the most proximal aspect of the greater trochanter and the most distal aspect of the lateral condyle. (**D**) Canal flare index was calculated as the ratio of the width of the femoral canal at the level of the lesser trochanter (red line) to the width of the femoral canal at the isthmus of the diaphysis (blue line). (**E**) Cranial/caudal tipping: angle between the long axis of the femur (red line) and the long axis of the implant stem (blue line). Caudal tipping was recorded as a positive value and cranial tipping was recorded as a negative value. (**F**) Medial/lateral tipping: angle between the long axis of the femur (red line) and the long axis of the implant stem (blue line). Varus/medial angulation was recorded as a negative value and valgus/lateral angulation was recorded as a positive value.

trochanter and in the femoral diaphysis distal to the lesser trochanter. Type 2 fit indicated that an implant made contact with the femoral cortex only proximal to or within the region of the lesser trochanter. Type 3 fit represented an implant that only made contact with the cortex in the femoral diaphysis distal to the lesser trochanter and, finally, type 4 fit indicated that an implant did not contact the femoral cortex at all.

Fracture Characterization

Fractures and fissures were characterized using post-failure radiographic analysis and side-by-side gross examination of the femurs. Post-failure femurs were photographed on cranial, caudal, medial and lateral planes and additional photographs of each fracture were taken. Type of failure was divided into four categories: pure subsidence, fissure, incomplete fracture and complete fracture. Any femur that completed the failure protocol without a radiographically or grossly detectable fissure or fracture line was classified as pure subsidence. Fissures were defined as cracks in the bone that did not extend completely through the cortex into the medullary cavity. Incomplete fractures were defined as cracks through the cortex of the bone that reached the medullary cavity, but did not result in completely separate pieces of bone. Any bone that had a fracture that travelled through cortex, medullary cavity and cortex again, thus

dividing the bone into separate pieces, was classified as a complete fracture. Fractures and fissures were characterized by their type, location and biomechanical mode of failure. The distal endpoint of the fissure/fracture was classified based on its location relative to the implant stem, and stability of the implant was evaluated by gross manipulation. Modes of failure consisted of torsion, which is indicated by a spiral fracture; compression, indicated by an oblique fracture; tension, which is signified by a transverse fracture; and combined bending and axial loading, which is reflected by a butterfly fracture.[23]

Statistical Analysis

A one-way analysis of variance was used to compare each radiographic measurement between the three groups to check for significant variations between the three implant groups, with the level of significance set at 0.05. Multiple regression analysis with at most six independent variables X was applied to each dependent variable in each implant type. The best explanatory variables for each dependent variable in each implant type were selected in a forward manner: each explanatory variable was added to the regression model one-by-one. All statistical analyses were done by RStudio ver. 1.1.453 for WIN (Boston, Massachusetts, United States). Significance and trend levels were set to be 0.05 and 0.10 respectively.

Results

The implant groups were classified as collarless, collared and lateral bolt. Each group consisted of $n = 6$ femurs, with three femurs implanted with a size 8 stem and three femurs implanted with a size 9 stem, except for the collared group, which had four femurs with a size 9 stem and only two with a size 8 stem. The CFI ranged from 1.78 to 2.60, with a mean ($\pm$ standard deviation) of 2.15 ± 0.20, and femoral length ranged from 182.5 to 207.4 mm with a mean of 195.9 mm $\pm$ 8.6 mm (►**Table 1**). For the collared group, the mean gap height from collar to calcar was 0.27 mm $\pm$ 0.25 mm, with a range of 0.00 to 0.68 mm. Measurements of size 8 stems at 5, 15 and 25 mm from the distal tip were recorded as a mean of 6.8 ± 0.1 mm, 7.8 ± 0.2 mm and 8.8 ± 0.2 mm on the CC projection and 6.3 ± 0.3 mm, 6.7 ± 0.4 mm and 7.3 ± 0.5 mm on the ML projection respectively. Measurements of size 9 stems at 5, 15 and 25 mm from the distal tip were recorded as a mean of 7.7 ± 0.1 mm, 8.7 ± 0.1 mm and 9.8 ± 0.2 mm on the CC projection, and 7.2 ± 0.3 mm, 7.6 ± 0.5 mm and 8.2 ± 0.6 mm on the ML projection respectively. Differences in the radiographic measurements between the three implant groups were not significant ($p > 0.05$).

Biomechanical and Radiographic Parameters

For both the loading and failure data, the collarless stem group had the highest number of significant effects of radiographic positioning parameters on the mechanical data (►**Tables 2–3**). For the loading data, the collared group had the fewest radiographic parameters that significantly affected biomechanical performance (►**Table 2**), and for the failure data the lateral bolt group had the fewest radiographic parameters that had a significant effect on the biomechanical performance (►**Table 3**).

During loading protocols, collarless stems that were seated relatively deeper within the canal had increased compressive stiffness ($p = 0.031$) and torsional stiffness ($p = 0.016$) during loading. Femurs with a lower CFI were found to have increased torsional stiffness ($p = 0.011$) with the collarless implants. Increased ML fill for the collarless implants was associated with a lower peak rotation ($p = 0.002$) and was the most significant association for the loading dataset, but increased CC fill ($p = 0.024$) and increased lateral angulation ($p = 0.021$) of the collarless stem were associated with a higher peak rotation. The collared group was the only other stem group to have an association with a significance level of $p < 0.05$ for the loading parameters: collared stems that were seated relatively lower within the femur had an increased peak displacement during loading ($p = 0.038$).

Biomechanical data from the failure protocols showed more significant effects from radiographic fit and fill parameters than the biomechanical data from the loading protocols did. Increased medial angulation of the distal implant stem for collarless implants showed increased torsional stiffness ($p = 0.003$), compressive stiffness ($p = 0.050$) and peak load ($p = 0.035$). Increased torsional stiffness of the lateral bolt stems, however, was associated with lateral angulation ($p = 0.001$). Increased lateral angulation ($p = 0.044$) and caudal angulation ($p = 0.024$) of the collarless stems was associated with an increased peak torque, and increased lateral

Table 1 Summary of the mean and range of each radiographic measurement

Variable	Collarless BFX		Collared BFX		Lateral bolt	
	Mean $\pm$ SD	Range	Mean $\pm$ SD	Range	Mean $\pm$ SD	Range
CFI	2.03 ± 0.19	1.78 to 2.28	2.13 ± 0.18	1.85 to 2.41	2.27 ± 0.20	2.00 to 2.60
ML stem angle (deg)	-1.1 ± 2.0	−3 to 2.6	0.6 ± 2.4	−2.6 to 2.4	-0.4 ± 2.8	−4.5 to 2.3
CC Stem angle (deg)	1.6 ± 2.4	−2.3 to 4.0	2.5 ± 2.4	−1.4 to 6.0	1.8 ± 1.8	−1.1 to 4.3
Average ML fill (%)	74.3 ± 4.7	66.9 to 79.9	75.6 ± 3.6	71.6 to 80.9	79.2 ± 9.8	70.7 to 96.6
Average CC fill (%)	61.1 ± 5.6	51.9 to 66.7	63 ± 6.7	55.6 to 72.8	69.3 ± 6.1	64.5 to 80.2
Stem level (normalized)	0.03 ± 0.01	0.02 to 0.04	0.04 ± 0.002	0.043 to 0.05	0.04 ± 0.01	0.03 to 0.05

Abbreviations: CC, craniocaudal; CFI, canal flare index; ML, mediolateral; SD, standard deviation.
Note: SD stands for standard deviation. CFI and stem level do not have units.

Table 2 Results of the regression analysis for gait loading

Mechanical loading variables	Collarless		Collared		Lateral bolt	
Radiographic variables	Coefficient ± SE	*p*-Value	Coefficient ± SE	*p*-Value	Coefficient ± SE	*p*-Value
Peak displacement (mm)						
Stem level			131.79 ± 43.07	0.038		
Compressive stiffness (kN/mm)						
Stem level	71.03 ± 21.69	0.031				
Peak rotation (deg)						
Average ML fill	−0.37 ± 0.02	0.002				
ML stem angle	0.26 ± 0.04	0.021				
Average CC fill	0.08 ± 0.01	0.024				
Torsional stiffness (Nm/deg)						
Canal flare index	−5.39 ± 0.97	0.011				
Stem level	111.58 ± 22.51	0.016				

Abbreviations: CC, craniocaudal; SE, standard error.
Note: Only radiographic variables with statistically significant correlations to the given biomechanical loading variables for one of more of the implant types are listed ($p < 0.05$). A negative coefficient value indicates a negative correlation between the radiographic and biomechanical variables for the given implant, while a positive coefficient indicates a positive correlation. SE represents standard error and *p* represents *p*-value. Shaded rows indicate the most clinically-relevant biomechanical variables. There were no correlations with $p < 0.05$ for the lateral bolt stems during loading protocols.

angulation was also associated with increased rotation at peak torque ($p = 0.05$). For collared stems, increased caudal angulation was associated with increased rotation at peak torque ($p = 0.023$) and increased displacement at peak load ($p = 0.013$). Increased CC fill for the collarless stems was associated with an increased peak load ($p = 0.010$) and an increased torsional stiffness (0.001). For the lateral bolt, however, increased torsional stiffness was associated with a decreased CC fill ($p = 0.007$). The ML fill was only significant for collared implants, as increased fill was associated with increased peak torque ($p = 0.043$). Increased CFI resulted in decreased torsional stiffness ($p = 0.006$) and increased peak load ($p = 0.023$) for the femurs with lateral bolt implants. In contrast, an increased CFI appeared to be associated with a decreased peak load ($p = 0.005$) for the collarless implants, as well as with a decreased compressive stiffness ($p = 0.039$) and increased peak torque ($p = 0.030$). Finally, collarless stems seated relatively deeper within the femoral canal were found to have a decreased rotation at peak torque ($p = 0.001$) and a decreased displacement at peak load ($p = 0.011$).

Several factors were trending toward, but did not reach significance ($0.05 < p < 0.10$). For loading data, these trending factors were CFI/peak displacement/collarless ($p = 0.062$), CFI/peak displacement/lateral bolt ($p = 0.067$) and CC stem angle/peak rotation/lateral bolt ($p = 0.073$). For failure data, the trending factors were average ML fill/peak load/collared ($p = 0.07$), average CC fill/displacement at peak load/collarless ($p = 0.082$), average CC fill/displacement at peak load/lateral bolt ($p = 0.086$), CC stem angle/compressive stiffness/collarless ($p = 0.073$) and ML stem angle/compressive stiffness/lateral bolt ($p = 0.084$).

Fractures and Implant Fit

Complete descriptive results from the fracture characterization and implant fit are displayed in ►**Table 4**. The majority of femurs had type 4 fit on both radiographic views; however, the lateral bolt implants had increased contact with the femoral cortex relative to the collarless and collared implants. No femurs failed with a complete fracture, and only one femur (collarless) failed from subsidence alone. The majority of femurs with collared and lateral bolt implants failed due to incomplete fractures, while most of the femurs with collarless implants failed due to fissures. A majority of the fractures and fissures spanned the metaphysis only, or travelled from the metaphysis to the mid-diaphysis. Half of the fracture or fissure lines that extended well beyond the distal implant tip were in the lateral bolt group. A majority of the fractures and fissures for the collarless and collared groups were oblique, while a majority of failure lines in the lateral bolt group were spiral.

Discussion

The results of this study show that, for the collarless implants, maximal compressive and torsional stiffness during loading protocols were achieved when stem level was maximized and CFI was minimized (►**Table 2**). During failure protocols, peak load was maximized when CFI was decreased, CC fill was increased and medial angulation was maximized (►**Table 3**). Also during failure protocols, peak torque was maximized by increased caudal angulation, CFI and lateral angulation (►**Table 3**). The collarless stems had the greatest peak torque when ML fill was maximized during failure protocols (►**Table 3**). The lateral bolt stems maximal peak load and torsional stiffness during failure protocols

Table 3 Results of the regression analysis for failure testing

Mechanical failure variables	Collarless		Collared		Lateral bolt	
Radiographic variables	**Coefficient ± SE**	***p*-Value**	**Coefficient ± SE**	***p*-Value**	**Coefficient ± SE**	***p*-Value**
Peak load (kN)						
Canal flare index	−3.09 ± 0.21	0.005			4.58 ± 1.27	0.023
Average CC fill	0.05 ± 0.01	0.01				
ML stem angle	−0.13 ± 0.02	0.035				
Displacement at peak load (mm)						
Stem level	−289.36 ± 51.72	0.011				
CC stem angle			0.21 ± 0.04	0.013		
Compressive stiffness (kN/mm)						
Canal flare index	−0.91 ± 0.18	0.039				
ML stem angle	−0.09 ± 0.02	0.05				
Peak torque (Nm)						
CC stem angle	0.36 ± 0.06	0.024				
Canal flare index	5.05 ± 0.91	0.031				
ML stem angle	0.48 ± 0.1	0.044				
Average ML fill			0.29 ± 0.1	0.043		
Rotation at peak torque (deg)						
Stem level	−824.98 ± 66.09	0.001				
ML stem angle	0.85 ± 0.27	0.05				
CC stem angle			0.53 ± 0.15	0.023		
Torsional stiffness (Nm/deg)						
Average CC fill	0.03 ± 0	0.001			−0.02 ± 0	0.007
ML stem angle	−0.05 ± 0.01	0.003			0.08 ± 0	0.001
Canal flare index					−0.51 ± 0.04	0.006

Abbreviations: CC, craniocaudal; ML, mediolateral; SE, standard error.
Note: Only radiographic variables with statistically significant correlations to the given biomechanical loading variables for one of more of the implant types are listed ($p < 0.05$). A negative coefficient value indicates a negative correlation between the radiographic and biomechanical variables for the given implant, while a positive coefficient indicates a positive correlation. SE represents standard error and p represents *p*-value. Shaded rows indicate the most clinically relevant biomechanical variables

when CC fill was decreased and CFI and lateral angulation of the distal implant tip were increased (►**Table 3**). In general, this study shows that the biomechanical performance of collarless stems is more influenced by the positioning of the stem within the femur than that of the other implant designs. This indicates that implant designs such as the collared stem or lateral bolt may allow for more variation in positioning before mechanical performance is compromised.

For the collarless stems, the opposite trends in CFI significance between several of the biomechanical variables during the loading and failure protocols are difficult to explain. However, this data may not accurately reflect the true performance of the collarless stem relative to the CFI of the femur since only one femur in this study could be considered to have a stovepipe morphology (CFI = 1.78). In previous studies, a CFI ≤ 1.8 has been associated with increased risk of implant failure and femoral fracture following implantation of the collarless stems, though a recent study found no significant correlation between CFI and stem complications.[10,17,21] It is possible that femurs with a stovepipe morphology allow more room for aberrant stem positioning during implantation, which could skew results during biomechanical studies. Similar to the conflicting CFI trends, opposite trends were also noted for the ML stem angle in this study; the benefits of minimizing lateral angulation of the distal stem tip have been demonstrated in several studies, which have shown that excessive angulation can lead to an increase in intraoperative fissure formation and increased strain.[21,24] In terms of general biomechanical performance, the collarless stems have been shown to be comparable to the lateral bolt and collared stems during both simulated gait loading and failure protocols.[18]

The collared and lateral bolt BFX stems were designed as alternatives to the standard collarless BFX stem to decrease subsidence and improve implant stability. Both stems have been shown to limit subsidence when compared with the collarless stem.[12,14] For the lateral bolt stems, increased CFI

Table 4 Descriptive characteristics of the femurs after failure testing and the postoperative implant fit characterizations

Fracture characterization										
Implant	**Femur**	**Failure type**	**Size**	**Shape**	**Proximal origin**	**Distal endpoint**	**Implant stability**	**ML stem fit**	**CC stem fit**	**Extension**
Collarless	1	B	A	C	M	M	A	4	4	A
	2	A	D	E	S	S	A	4	4	No fracture
	3	B	B	A	M	CdM	B	3	4	B
	4	B	A	D	CrM	CrM	A	4	4	A
	5	C	B	A	M	CdM	A	2	4	B
	6	C	C	A	M	CdM	A	4	3	C
Collared	1	C	B	A	M	Cd	A	4	4	B
	2	C	B	A	M	CdM	C	4	3	B
	3	C	B	D	M	CdM	A	4	4	B
	4	C	B	A	CrM	CdM	A	4	4	B
	5	C	B	A	CrM	CdM	C	3	4	B
	6	C	C	D	M	M	A	4	1	C
Lateral bolt	1	C	A	A	CdM	CdM	A	4	4	A
	2	B	A	C	M	M	A	4	1	B
	3	C	B	B	M	Cd	C	4	2	B
	4	C	A	A	CdL	CdL	A	3	4	A
	5	C	C	B	M	Cd, L	A	3	3	C
	6	C	C	B	M	Cr	A	4	2	C
Key:										
Failure type: (A) Pure subsidence, (B) fissure, (C) incomplete fracture										
Size: Longitudinal distance that the fracture/fissure spans on the bone. (A) Metaphyseal only, (B) metaphysis to mid-diaphysis, (C) metaphysis to distal half of diaphysis, (D) no fracture or fissure present										
Shape: Shape of fracture or fissure. (A) Oblique, (B) spiral, (C) longitudinal, (D) butterfly, (E) no fracture or fissure present										
Proximal origin: Surface of the femur on which the most proximal section of the fracture/fissure is located. (Cr) cranial, (CrM) craniomedial, (M) medial, (CdM) caudomedial, (Cd) caudal, (CdL) caudolateral, (L) lateral, (CrL) craniolateral										
Distal endpoint: Surface of the femur on which the most distal section of the fracture/fissure is located. (Cr) cranial, (CrM) craniomedial, (M) medial, (CdM) caudomedial, (Cd) caudal, (CdL) caudolateral, (L) lateral, (CrL) craniolateral										
Implant stability: Stability of implant within the bone, post-failure. (A) Stable; (B) mildly loose, movement of less than or equal to 0.5mm when pushed back-and-forth; (C) moderately loose, movement of greater than 0.5mm when pushed back-and-forth; (D) implant no longer in bone or can be removed from bone										
CC and ML stem fit: Assessment of implant contact with bone craniocaudally (CC) and mediolaterally (ML) immediately post-implantation. (1) Implant makes contact with femoral cortex in both the metaphyseal/trochanteric region and the diaphyseal region, (2) implant only makes contact with femoral cortex in the metaphyseal/trochanteric region, (3) implant only makes contact with femoral cortex in diaphyseal region, (4) implant does not make contact with femoral cortex										
Extension: Description of distal extension of fracture/fissure relative to the implant stem. (A) Extends only through proximal metaphyseal/trochanteric region, (B) extends into the proximal diaphysis, no further than the level of the stem tip, (C) extends far distal to the stem tip										

Abbreviations: CC, craniocaudal; ML, mediolateral.

resulted in a greater peak load, but also caused a decreased torsional stiffness; this could be explained by the presence of the interlocking bolt, which is intended to increase resistance to subsidence and rotation during the early postoperative period, but has been suspected to cause increased shearing forces during torsion, potentially leading to an increased risk of torsional failure.[12] Fracture data from this study supports this suspicion (►**Table 4**). Additionally, during failure protocols the lateral bolt stems had a significantly greater peak torque and rotation at peak torque relative to the collarless and collared implants, and a greater torsional stiffness than the collarless stems ($p < 0.05$).[18] Based on these findings, it is likely that, while the lateral bolt stem was capable of withstanding greater torque, the large torsional force was still transferred from the stem to the bone at the bone–implant interface between the lateral bolt and the

lateral cortex. Because the bolt is meant to limit rotation of the stem within the femoral canal, it may behave similarly to an interlocking nail in that shearing forces originating at the exit hole for the lateral bolt are transmitted to the lateral cortex and contribute to torsional failure, as predicted in a previous study.[12]

There is currently a lack of data comparing the radiographic fit and fill of collared stems with their biomechanical performance in veterinary medicine. Research on human total hip implants has shown that collared stems are capable of withstanding larger vertical and horizontal forces than collarless stems before the occurrence of subsidence or fracture.[25] In veterinary biomechanical research, the collared implants were shown to have greater torsional stiffness and decreased displacement at failure when compared with the collarless implants ($p < 0.05$); however, the peak loads for these two implant groups were not significantly different ($p > 0.05$).[18] While this study found that increased ML fill was correlated with an increased peak load for collared stems, CFI and canal fill were not found to influence risk of subsidence for collared stems in humans.[26] The biomechanical data for the collared group in this study may have been impacted, however, by small gaps between the collar and calcar; stems that are not seated with the collar in direct contact with the calcar will experience a limited amount of subsidence that closes the small gap during loading.[14,18] However, no collared implants in this study had a measured gap of > 0.68 mm, and all gaps between the collar and calcar were likely closed during loading protocols. Previous research has demonstrated that collar to calcar gaps of up to 3 mm can experience postoperative gap closure with no associated, clinically relevant complications, and that study also reported a collar-to-calcar-gap prevalence of ~82% in implanted collared stems.[14] Furthermore, according to implantation guidelines for the collared stems, it is preferable to have a collar–calcar gap of 0.5 to 1.5 mm after impaction.[19] Therefore, while the gaps may have influenced the biomechanical performance of the collared stems, these results may still be an accurate representation, as many collared stems implanted in clinical practice will initially have small gaps present between the collar and calcar.

The results of this study also show that there were more radiographic factors that had a significant impact on the biomechanical performance of the stems during supraphysiological loading than during normal gait loading (►**Tables 2** and **3**). This finding is similar to the results of a separate study's comparison of biomechanical data between implant groups, which also showed a larger number of significant differences in the biomechanical performance between implant groups under the supraphysiological (failure) gait protocols than under simulated gait loading protocols.[18] Supraphysiological loading has been documented in human hip replacements, where studies have shown that stumbling can generate peak forces up to two times greater than normal loading forces, and it is likely that similar supraphysiological loading conditions occur in canine patients, as well.[27] As a result, improving the biomechanical performance of these implants at supraphysiological loads would have a positive impact on postoperative implant behaviour.

For all three implant groups, the most common fracture location was on the medial surface, originating from the medial calcar, which supports findings from various other studies that note that acute subsidence leads to expansion of the femoral cortex and subsequent fractures originating from the medial calcar.[10,12,17,21,28] Both the collarless and collared groups most commonly failed with oblique fissures and fractures, indicating that the failure is likely due to compression. Interestingly, past research has shown that a majority of intraoperative fissures were longitudinal when only axial loading was evaluated.[29] The oblique geometry of the fissures and fractures found in this study is likely attributed to the addition of a torsional loading component. The lateral bolt implant group most commonly failed with spiral fractures, likely due to the increased shearing forces during torsion caused by the bolt exiting the lateral cortex.[12] The majority of the implants remained stable in the bone after fracturing, but very few implants in this study actually made contact with the femoral cortex after implantation. Research in human total hip replacements indicates that increased contact between the stem and the femoral cortex is associated with greater initial stability and a reduced incidence of subsidence, likely due to a wider distribution of stress across the femoral cortex.[22] In veterinary research, however, overall canal fill has not been shown to impact subsidence or risk of postoperative femoral fracture.[17,21,28]

Limitations of this study include the small sample size and the *ex vivo* design. The femurs used for the study were limited by the availability of appropriately sourced cadavers, which resulted in the small sample size and the relatively wide range of CFI measurements. Because this study examined the mechanical performance of these implants in cadaveric femurs, it does not reflect the impact of bony ingrowth, bone healing and bone remodelling over time on the implants. This study is also unable to analyse the long-term effects of implantation on the patient, including comfort, return to function and longevity of the implant systems. In addition, because this study primarily used canine femurs with a CFI ≥ 1.8, it did not address the increased risk of fractures and subsidence associated with stovepipe femurs.[10,17] The collar modification to the standard BFX stem has previously been shown to limit stem subsidence in femurs with the stovepipe morphology.[14] It is also possible that differences in femur positioning may have affected the accuracy of the radiographic measurements; changes in the positioning of the femur on the film cassette have been shown to affect the perceived position of the implant within the femur in cemented stems; however, measurements of stem angulation were likely not significantly affected.[30,31] Radiographic assessment was also found to be less accurate than three-dimensional measurements obtained using computed tomography for evaluating CFI.[32] Some radiographic measurements may also have been inconsistent due to human error. Finally, the learning curve for total hip replacements may have impacted

positioning of implants in this study.[33] However, postoperative radiographs were used to confirm proper implant position in an effort to minimize this potential source of error.

This study demonstrated that the biomechanical performance of collarless stems is more affected by implant positioning when compared with that of the augmented designs. CFI, stem level, canal fill and stem angle all influenced the biomechanical performance of the implants to some degree. Data from this study supported the suggestion that the lateral bolt may contribute to increased shearing forces during torsion. Furthermore, based on the fracture analysis, the addition of the collar did not alter the typical mode of failure (compression) of the standard collarless stem. Future directions could include the use of simulated gait protocols to compare the performance of the lateral bolt and collared implants in femurs with a stovepipe morphology (CFI < 1.8), or further investigation into the performance of other novel implant designs and their long-term outcomes in canine patients.

Authors' Contributions

N.J.W. and K.J.A. contributed to conception of study, study design, data acquisition, data analysis, interpretation of results and drafting of the submitted manuscript. N.R.O. and M.A.M. contributed to conception of study, study design and the acquisition, analysis and interpretation of biomechanical data. K.A.M. contributed to the conception, design and analysis and interpretation of data for biomechanical testing. G.M.V. and R.H. contributed to conception of study and implantation of stems. K.J.A. contributed to implantation of stems. D.M.V. contributed to study design and interpretation of data. M.K. contributed to analysis and interpretation of data. K.H. contributed to conception of study, study design and interpretation of data. All authors revised and approved the submitted manuscript.

Funding

None.

Conflict of Interest

None declared.

Acknowledgements

We would like to thank Mizuki Tomihari for his work on the statistical analysis and BioMedtrix for donating the implants used in this study.

References

1 Kalis RH, Liska WD, Jankovits DA. Total hip replacement as a treatment option for capital physeal fractures in dogs and cats. Vet Surg 2012;41(01):148–155
2 Jankovits DA, Liska WD, Kalis RH. Treatment of avascular necrosis of the femoral head in small dogs with micro total hip replacement. Vet Surg 2012;41(01):143–147
3 Lascelles BD, Freire M, Roe SC, DePuy V, Smith E, Marcellin-Little DJ. Evaluation of functional outcome after BFX total hip replacement using a pressure sensitive walkway. Vet Surg 2010;39(01):71–77
4 Peck JN, Liska WD, DeYoung DJ, Marcellin-Little DJ. Clinical application of total hip replacement. In: Peck JN, Marcellin-Little DJ, eds. Advances in small animal total joint replacement. Ames: Wiley-Blackwell; 2013:69–107
5 Scherrer W, Holsworth I, Goossens M, Schulz K. Coxofemoral arthroscopy and total hip arthroplasty for management of intermediate grade fibrosarcoma in a dog. Vet Surg 2005;34(01): 43–46
6 Trostel CD, Peck JN, deHaan JJ. Spontaneous bilateral coxofemoral luxation in four dogs. J Am Anim Hosp Assoc 2000;36(03): 268–276
7 Mitchell EP, Marcellin-Little DM. Radiographic assessment of short term stability of uncemented femoral stems. Vet Surg 2005;34:E20(abstr)
8 Szmukler-Moncler S, Salama H, Reingewirtz Y, Dubruille JH. Timing of loading and effect of micromotion on bone-dental implant interface: review of experimental literature. J Biomed Mater Res 1998;43(02):192–203
9 Brunski JB. Biomaterials and biomechanics in dental implant design. Int J Oral Maxillofac Implants 1988;3(02):85–97
10 Rashmir-Raven AM, DeYoung DJ, Abrams CF Jr, Aberman HA, Richardson DC. Subsidence of an uncemented canine femoral stem. Vet Surg 1992;21(05):327–331
11 Kidd SW, Preston CA, Moore GE. Complications of porous-coated press-fit cementless total hip replacement in dogs. Vet Comp Orthop Traumatol 2016;29(05):402–408
12 Buks Y, Wendelburg KL, Stover SM, Garcia-Nolen TC. The effects of interlocking a universal hip cementless stem on implant subsidence and mechanical properties of cadaveric canine femora. Vet Surg 2016;45(02):155–164
13 Dosch M, Hayashi K, Garcia TC, Weeren R, Stover SM. Biomechanical evaluation of the helica femoral implant system using traditional and modified techniques. Vet Surg 2013;42 (07):867–876
14 Liska WD, Doyle ND. Use of an electron beam melting manufactured titanium collared cementless femoral stem to resist subsidence after canine total hip replacement. Vet Surg 2015;44(07): 883–894
15 Pozzi A, Peck JN, Chao P, Choate CJ, Barousse D, Conrad B. Mechanical evaluation of adjunctive fixation for prevention of periprosthetic femur fracture with the Zurich cementless total hip prosthesis. Vet Surg 2013;42(05):529–534
16 Page AE, Allan C, Jasty M, Harrigan TP, Bragdon CR, Harris WH. Determination of loading parameters in the canine hip in vivo. J Biomech 1993;26(4-5):571–579
17 Ganz SM, Jackson J, VanEnkevort B. Risk factors for femoral fracture after canine press-fit cementless total hip arthroplasty. Vet Surg 2010;39(06):688–695
18 Ordway NR, Ash KJ, Miller MA, Mann KA, Hayashi K. A biomechanical comparison of four hip arthroplasty designs in a canine model. Vet Comp Orthop Traumatol 2019;32(05):369–375
19 Liska WD. BFX ® EBM Titanium Collared Femoral Stem: Surgical Technique Details. Houston: Global Veterinary Specialists PLLC; 2017:4–5. Available at: https://biomedtrix.com/bfx-ebm-collared-stem/. Accessed February 2, 2020
20 BioMedtrix. BFX ® Lateral Bolt System Surgical Technique. Whippany: BioMedtrix:1–9. Available at: https://biomedtrix.com/bfx-ebm-lateral-bolt-stem/. Accessed June 12, 2020
21 Townsend S, Kim SE, Pozzi A. Effect of stem sizing and position on short-term complications with canine press fit cementless total hip arthroplasty. Vet Surg 2017;46(06):803–811
22 Issa K, Pivec R, Wuestemann T, Tatevossian T, Nevelos J, Mont MA. Radiographic fit and fill analysis of a new second-generation proximally coated cementless stem compared to its predicate design. J Arthroplasty 2014;29(01):192–198
23 Browner BD, Jupiter JB, Levine AM, Trafton PG. Skeletal Trauma: Fractures, Dislocations, Ligamentous Injuries. Vol 1. 2nd ed. Philadelphia, PA: Saunders; 1998:51–82

24 Pernell RT, Gross RS, Milton JL, et al. Femoral strain distribution and subsidence after physiological loading of a cementless canine femoral prosthesis: the effects of implant orientation, canal fill, and implant fit. Vet Surg 1994;23(06):503–518
25 Demey G, Fary C, Lustig S, Neyret P, si Selmi TA. Does a collar improve the immediate stability of uncemented femoral hip stems in total hip arthroplasty? A bilateral comparative cadaver study. J Arthroplasty 2011;26(08):1549–1555
26 Ries C, Boese CK, Dietrich F, Miehlke W, Heisel C. Femoral stem subsidence in cementless total hip arthroplasty: a retrospective single-centre study. Int Orthop 2019;43(02):307–314
27 Bergmann G, Graichen F, Rohlmann A. Hip joint contact forces during stumbling. Langenbecks Arch Surg 2004;389(01): 53–59
28 Townsend KL, Kowaleski MP, Johnson KA Initial Stability and Femoral Strain Pattern during Axial Loading of Canine Cementless Femoral Prostheses: Effect of Resection Level and Implant Size. In: Proceedings of the 34th Annual Conference of the Veterinary Orthopedic Society; Sun Valley, Idaho; March 3–10, 2007
29 McCulloch RS, Roe SC, Marcellin-Little DJ, Mente PL. Resistance to subsidence of an uncemented femoral stem after cerclage wiring of a fissure. Vet Surg 2012;41(01):163–167
30 Jehn CT, Manley PA. The effects of femur and implant position on the radiographic assessment of total hip femoral implants in dogs. Vet Surg 2002;31(04):349–357
31 Jehn CT, Bergh MS, Manley PA. Orthogonal view analysis for evaluating the femoral component position of total hip implants in dogs using postoperative radiographs. Vet Surg 2003;32(02):134–141
32 Husmann O, Rubin PJ, Leyvraz PF, de Roguin B, Argenson JN. Three-dimensional morphology of the proximal femur. J Arthroplasty 1997;12(04):444–450
33 de Steiger RN, Lorimer M, Solomon M. What is the learning curve for the anterior approach for total hip arthroplasty? Clin Orthop Relat Res 2015;473(12):3860–3866